

ROSAT EVIDENCE FOR INTRINSIC OXYGEN ABSORPTION IN COOLING FLOW GALAXIES AND GROUPS

DAVID A. BUOTE¹

UCO/Lick Observatory, University of California at Santa Cruz, Santa Cruz, CA 95064; buote@ucolick.org

Accepted for Publication in The Astrophysical Journal

ABSTRACT

The existence of large quantities of gas that have cooled and dropped out of the hot phase in massive elliptical galaxies, groups, and clusters is the key prediction of the inhomogeneous cooling flow scenario. Using spatially resolved, deprojected *ROSAT* PSPC spectra of 10 of the brightest cooling flow galaxies and groups with low Galactic column densities we have detected intrinsic absorption over energies $\sim 0.4 - 0.8$ keV at the $2\sigma/3\sigma$ level in half of the sample. Since no intrinsic absorption is indicated for energies below ~ 0.4 keV, the most reasonable model for the absorber is collisionally ionized gas at temperatures $T = 10^{5-6}$ K with most of the absorption arising from ionized states of oxygen but with a significant contribution from carbon and nitrogen. The soft X-ray emission of this warm gas can also explain the sub-Galactic column densities of cold gas inferred within the central regions of most of the systems. (This could not be explained by an absorber composed only of dust.) Attributing the absorption to ionized gas reconciles the large columns of cold H and He inferred from *Einstein* and *ASCA* with the lack of such columns inferred from *ROSAT*.

Within the central $\sim 10 - 20$ kpc, where the constraints are most secure, the mass of the ionized absorber is consistent with most (perhaps all) of the matter deposited by a cooling flow over the lifetime of the flow. Since the warm absorber produces no significant H or He absorption the large absorber masses are consistent with the negligible atomic and molecular H inferred from H₁ and CO observations of cooling flows. It is also found that if $T \gtrsim 2 \times 10^5$ K then the optical and FUV emission implied by the warm gas does not violate published constraints. An important theoretical challenge is to understand how the warm temperature is maintained and how the gas is supported gravitationally, and we discuss possible solutions to these problems that would require fundamental modification of the standard cooling flow scenario. Finally, we discuss how the prediction of warm ionized gas as the product of mass drop-out in these and other cooling flows can be verified with new *Chandra* and *XMM* observations.

Subject headings: cooling flows – intergalactic medium – X-rays: galaxies

1. INTRODUCTION

The evolution of the hot gas in the centers of massive elliptical galaxies, groups, and galaxy clusters has been most frequently interpreted in terms of the cooling flow paradigm (e.g., Fabian 1994). However, the characteristic radially increasing temperature profiles and centrally peaked X-ray surface brightness profiles usually attributed to cooling flows can be successfully described by only assuming a two-tier structure for the gravitational potential (e.g., Ikebe et al 1996; Xu et al 1998); i.e., the cooler gas sits in the shallower potential associated with the central galaxy whereas the hotter gas sits in the deeper potential of the surrounding group or cluster. The two-tier structure is typically incorporated into cooling flow models (e.g., Thomas, Fabian, & Nulsen 1987; Brighenti & Mathews 1998), but since cooling flows are not necessarily required to explain the temperatures and surface brightness profiles of the hot gas why should they still receive attention?

Unlike the empirical two-tier potential model, cooling flows attempt to offer a nearly complete theoretical description of the time evolution of the gas properties. A cooling flow describes the dynamical evolution and the X-ray emission of the hot gas by considering the following simple picture for the energy balance of a parcel of gas. Since the parcel of gas emits X-rays it loses energy. As the

parcel radiates it sinks deeper (i.e., flows inward) into the potential well of the system where it encounters regions of higher density and therefore higher pressure. Consequently, the gas parcel contracts but is then heated as the result of PdV work. This balance between cooling and heating is expected to apply over much of the cooling flow. Within the central regions of highest density this balance is broken as cooling overwhelms the heating leading to the key prediction of the inhomogeneous cooling flow scenario: in massive elliptical galaxies, groups, and clusters large quantities of gas should have cooled and dropped out of the flow and be distributed at least over the central regions of the flow.

This prediction has inspired many searches in H₁ and CO for cold gas at the centers of cooling flows, and all such attempts have either detected small gas masses or placed upper limits which are in embarrassing disagreement with the large masses expected to have been deposited in a cooling flow (e.g., Bregman, Hogg, & Roberts 1992; O’Dea et al 1994). If instead the mass drop-out is in the form of dust then current constraints on the infrared emission in cluster cores are not inconsistent with cooling flow models (e.g., Voit & Donahue 1995; Allen et al 2000b). But cooling flows are not required to explain the infrared data in clusters (Lester et al, 1995) and individual elliptical galax-

¹Chandra Fellow

ies (Tsai & Mathews, 1996).

The case for mass drop-out received a substantial boost with the discovery of intrinsic soft X-ray absorption in the *Einstein* spectral data of cooling flow clusters (White et al 1991; Johnstone et al 1992). The *Einstein* results have been verified with multitemperature models of the *ASCA* spectral data of clusters (Fabian et al 1994; Allen et al 2000b), elliptical galaxies, and groups (Buote & Fabian 1998; Buote 1999, 2000a; Allen et al 2000a). If the soft X-ray absorption is interpreted as cold gas then the large intrinsic column densities of cold H suggested by the *Einstein* and *ASCA* observations still suffer from the tremendous disagreement with the H I and CO observations noted above. The *Einstein* and *ASCA* results appear even more suspect when considering that in systems with low Galactic columns (where any intrinsic absorption should be easier to detect) no significant excess absorption from cold gas is ever found with the *ROSAT* PSPC which should be more sensitive to the absorption because of its softer bandpass, 0.1-2.4 keV (e.g., David et al 1994; Jones et al 1997; Briel & Henry 1996).

We have re-examined the *ROSAT* PSPC data of cooling flows to search for evidence of intrinsic soft X-ray absorption and in particular have allowed for the possibility that the absorber is not cold. Previously in Buote (2000c; hereafter PAPER2) we have presented temperature and metallicity profiles of the hot gas in 10 of the brightest cooling flow galaxies and groups inferred from deprojection analysis of the PSPC data. We refer the reader to that paper for details on the data reduction and deprojection procedure.

In this paper we present the absorption profiles of the 10 galaxies and groups, each of which have low Galactic column densities (see Table 1 of PAPER2). Partial results for two systems analyzed in the present paper (NGC 1399 and 5044) also appear with results for the cluster A1795 in Buote (2000b; hereafter PAPER1). In §2 we describe the models used to parameterize the soft X-ray absorption. We present the radial absorption profiles for a standard absorber model with solar abundances in §3.1. The effects of partial covering and the sensitivity of the results to the bandpass are discussed in §3.2 and §3.3. The results of modeling the absorption with an oxygen edge are presented in §3.4. In §3.6 we consider multiphase models such as cooling flows (§3.6.1). Evidence for emission from a warm gaseous component is described in §3.6.3. We demonstrate the consistency of the *ROSAT* and *ASCA* absorption measurements in §4. In §5 we discuss in detail the implications of our absorption measurements for the physical state of the absorber, the cooling flow scenario, observations at other wavelengths, and theoretical models. Finally, in §6 we present our conclusions and discuss prospects for verifying our prediction of warm ionized gas in cooling flows with future X-ray observations.

2. MODELS

2.1. Hot Plasma

As discussed in PAPER2 we use the MEKAL plasma code to represent the emission from a single temperature component of hot gas. Because of the limited energy resolution of *ROSAT* we initially focus on a “single phase” representation of the hot gas such that a single temperature component exists within each three-dimensional ra-

dial annulus. Multiphase models are examined in §3.6.

2.2. Absorber

It is standard practice to represent the soft X-ray absorption arising from the Milky Way by material with solar abundances distributed as a foreground screen at zero redshift. In this standard absorption model the X-ray flux is diminished according to $A(E) = \exp(-N_{\text{H}}\sigma(E))$, where N_{H} is the hydrogen column density and $\sigma(E)$ is the energy-dependent photo-electric absorption cross section for an absorber with solar abundances. We allow N_{H} to be a free parameter in our fits to indicate any excess absorption intrinsic to a galaxy or group and also to allow for any errors in the assumed Galactic value for N_{H} and for any calibration uncertainties. Note that in this standard model N_{H} is measured as a function of two-dimensional radius, R , on the sky.

Intrinsic absorption is expressed more generally as,

$$A(E) = f \exp(-N_{\text{H}}\sigma[E(1+z)]) + (1-f),$$

where z is the source redshift and f is the covering factor. Since the redshifts are small for the objects in our sample any absorption in excess of the Galactic value indicated by the standard model is essentially that of an intrinsic absorber with $f = 1$ placed in front of the source. We discuss the effects of $f < 1$ in §3.2.

As discussed in PAPER1 we consider oxygen absorption intrinsic to the galaxy or group which we represent by the simple parameterization of an edge, $\exp[-\tau(E/E_0)^{-3}]$ for $E \geq E_0$, where E_0 is the energy of the edge in the rest frame of the galaxy or group, and τ is the optical depth. To facilitate a consistent comparison to the standard absorber model we place this edge in front of the source, and thus τ is also measured as a function of two-dimensional radius, R , on the sky. Models with $f < 1$ behave similarly to the solar-abundance absorber (§3.2).

The photo-electric absorption cross sections used in this paper are given by Balucińska-Church & McCammon (1992). Although Arabadjis & Bregman (1999) point out that the He cross section at 0.15 keV is in error by 13%, since we analyze $E > 0.2$ keV we find that our fits do not change when using the Morrison & McCammon (1983) cross sections which have the correct He value. Further details on the spectral models used in the analysis are given in PAPER2.

3. RADIAL ABSORPTION PROFILES

Following PAPER2 we plot in Figures 1-4 the radial profiles of the column density and oxygen edge optical depth obtained from the deprojection analysis according to the number of annuli for which useful constraints on the parameters were obtained. This categorizes the systems essentially according to the S/N of the data. We refer the reader to PAPER2 for the temperature and metallicity profiles corresponding to these models.

In several cases the column densities and optical depths could not be constrained in the outermost annuli. Owing to the nature of the deprojection method large errors in the outer annuli can significantly bias the results for nearby inner annuli. Hence, in some systems we fixed the column densities to their nominal Galactic values or the edge optical depths to zero in the relevant outer annuli.

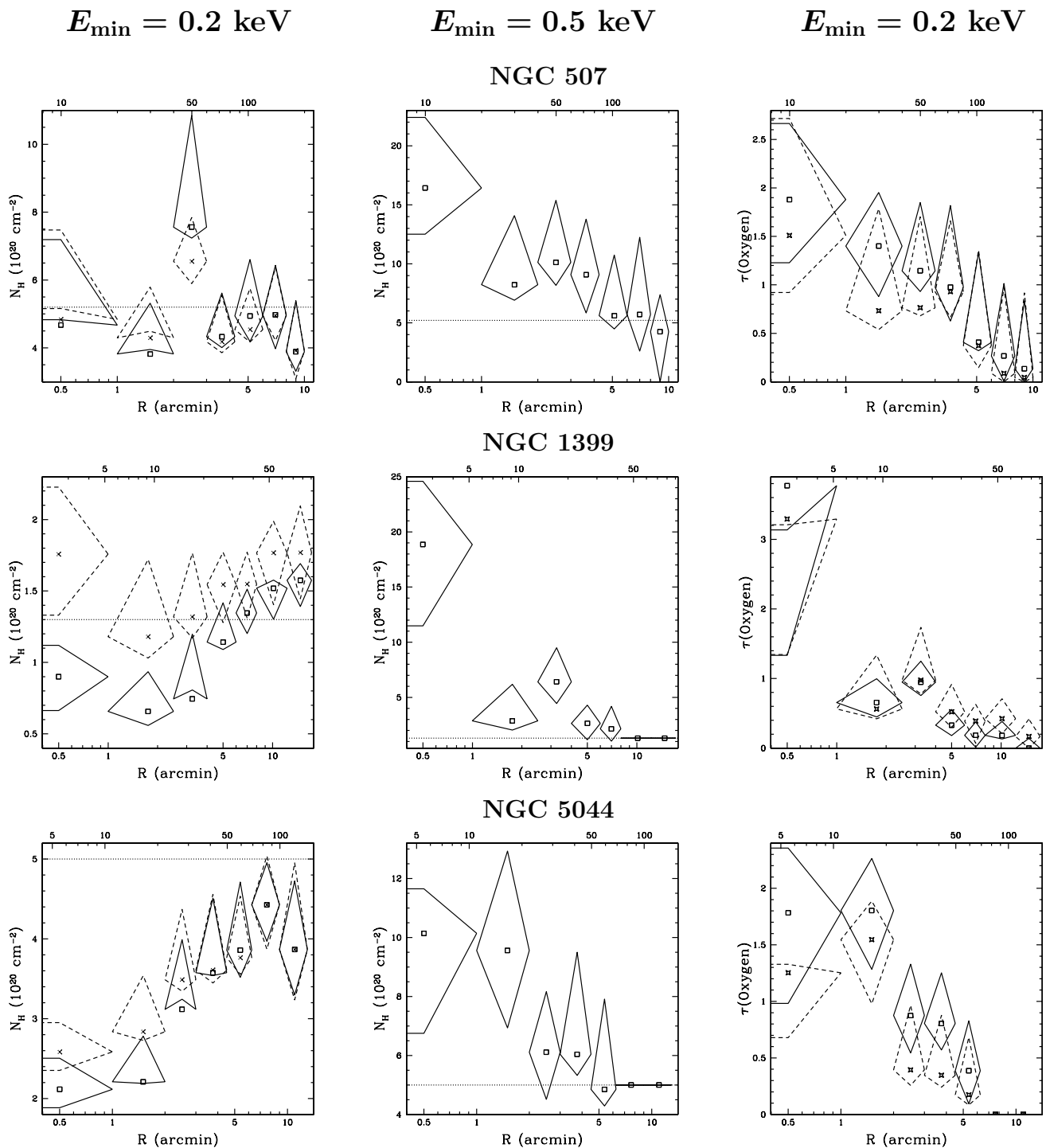


FIG. 1.— Results of the deprojection analysis for the systems where interesting constraints were obtained in 7 annuli. (Left panels) The column density profiles for a standard foreground absorber with solar abundances obtained from fits over 0.2-2.2 keV (i.e., $E_{\min} = 0.2$ keV) are denoted by open squares for best fit and solid diamonds for 1σ error bars; models which also have an intrinsic oxygen edge are represented by crosses and dashed diamonds. The Galactic hydrogen column density (Dickey & Lockman, 1990) is shown as a dotted line. Radial units are arcminutes on the bottom axis and kpc on the top. (Middle panels) The column density profiles for a standard absorber obtained from fits over 0.5-2.2 keV (i.e., $E_{\min} = 0.5$ keV). (Right panels) Optical depths for an oxygen edge at 0.532 keV (rest frame) obtained from fits with $E_{\min} = 0.2$ keV. The open squares and solid diamonds are respectively the best fit and 1σ errors for models where the standard absorber has N_{H} fixed to the Galactic value; crosses and dashed diamonds refer to models with variable N_{H} and thus correspond to similarly marked models in the left panels.

3.1. Foreground Absorber with Solar Abundances

We begin by examining the spectral fits using the standard absorption model of a foreground screen ($z = 0$) with solar abundances. The left panels of Figures 1-4 show

$N_{\text{H}}(R)$ obtained from spectral fits over the energy range 0.2-2.2 keV. Our column density profiles are consistent with those presented in previous *ROSAT* studies (Forman et al 1993; David et al 1994; Trinchieri et al 1994; Kim

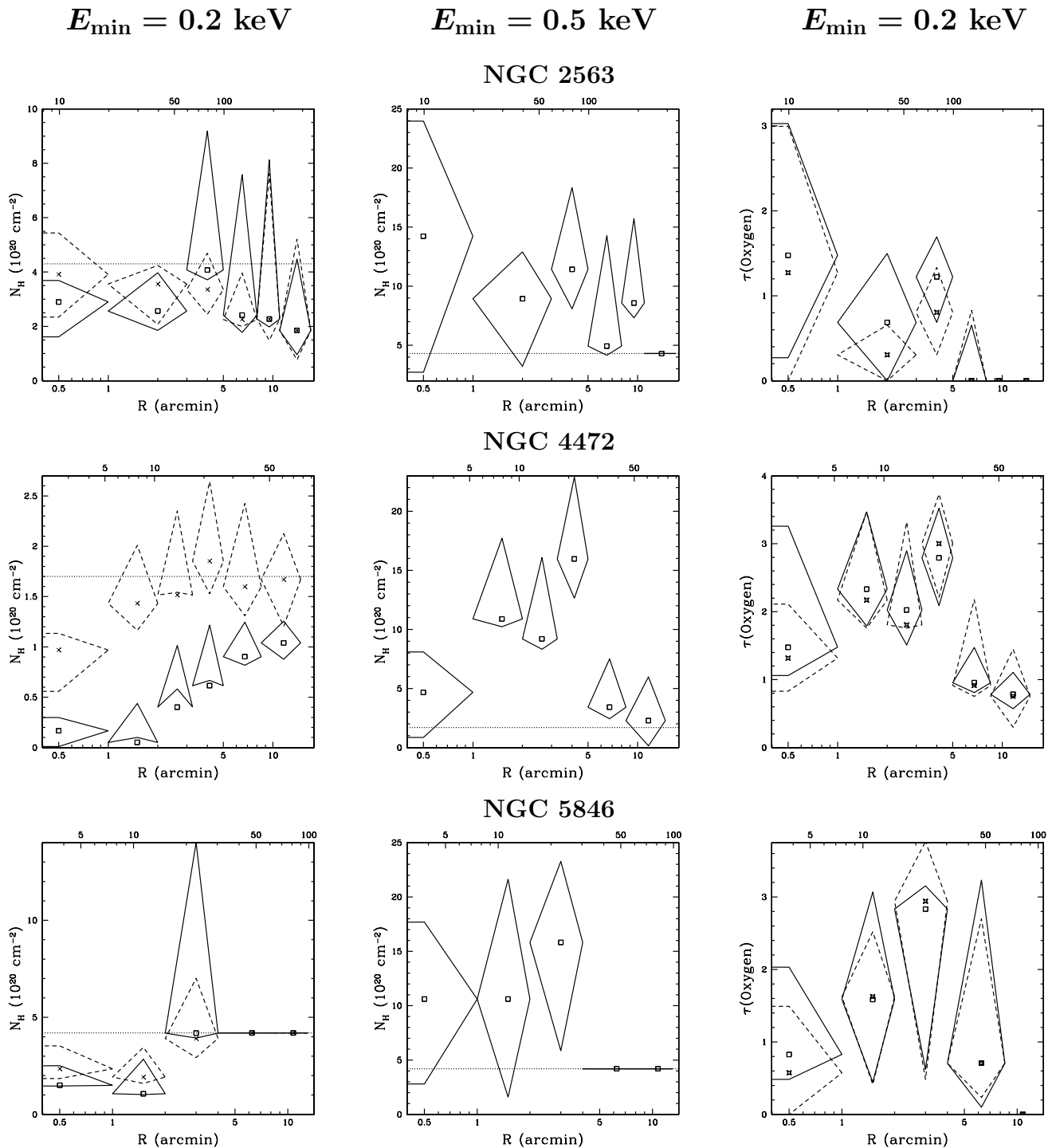


FIG. 2.— As Figure 1 but for systems with 5 or 6 annuli.

& Fabbiano 1995; Jones et al 1997; Trinchieri et al 1997; Buote 1999) after accounting for the different plasma codes and solar abundances used.

The column densities are always within a factor of ~ 2 of the Galactic value ($N_{\text{H}}^{\text{Gal}}$), though in most cases N_{H} decreases as R decreases such that $N_{\text{H}} < N_{\text{H}}^{\text{Gal}}$ at small R . The quality of the fits for four of these systems is also formally poor ($P < 0.01$) in the central $1'$ bin (Table 1), and for several objects in the sample the metallicities are

very large and very inconsistent with all ASCA studies (see PAPER2).² Since $N_{\text{H}} \sim N_{\text{H}}^{\text{Gal}}$ in the outer radii the observation that $N_{\text{H}} < N_{\text{H}}^{\text{Gal}}$ at small R indicates that, whatever the origin of the deficit, it must be intrinsic to the source. (We provide an explanation in §3.6.3.)

The approximately Galactic columns are wholly inconsistent with the large excess columns inferred from multitemperature models of the spatially integrated ASCA

²Here P represents the χ^2 null hypothesis probability under the assumption of gaussian random errors. We discuss the suitability of this approximation for interpreting goodness of fit in section 3.4 of PAPER2.

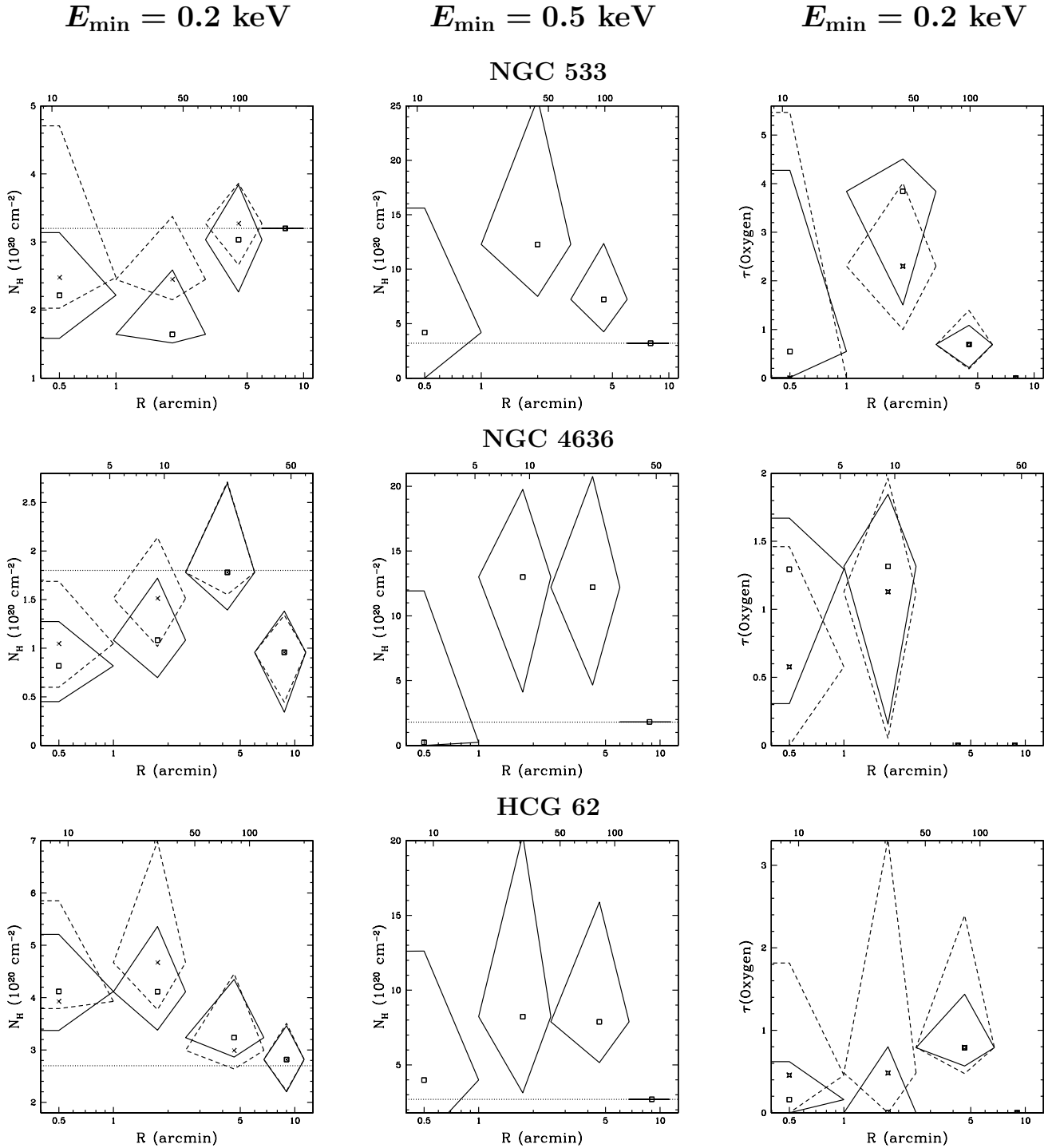


FIG. 3.— As Figure 1 but for systems with 4 annuli.

spectral data of these systems (Buote & Fabian 1998; Buote 1999, 2000a; Allen et al 2000a). We now address the origin of this inconsistency.

3.2. Effects of Partial Covering

It has been suggested that the reason why analyses with the PSPC do not infer large excess column densities for cluster cooling flows is that the standard foreground model used above systematically underestimates the true column intrinsic to the system (Allen & Fabian 1996; Sarazin, Wise, & Markevitch 1998). However, in

PAPER1 we have tested this hypothesis for NGC 1399 and 5044 (and the cluster A1795) using our deprojection code. We find that the hot gas within the central $r = 1'$ (3D) cannot be absorbed very differently from the gas projected from larger radii because their spectral shapes for energies below ~ 0.5 keV are very similar. If we do assume an absorber with covering factor $f = 0.5$ we obtain an excess column $\Delta N_{\text{H}} = 0$ at best fit and $\Delta N_{\text{H}} < N_{\text{H}}^{\text{Gal}}$ at $> 90\%$ confidence for NGC 1399 and 5044. (Note that the $f = 0.5$ model implies a flat absorbing screen that bisects the source so that the 2D and 3D radii are equal, and thus

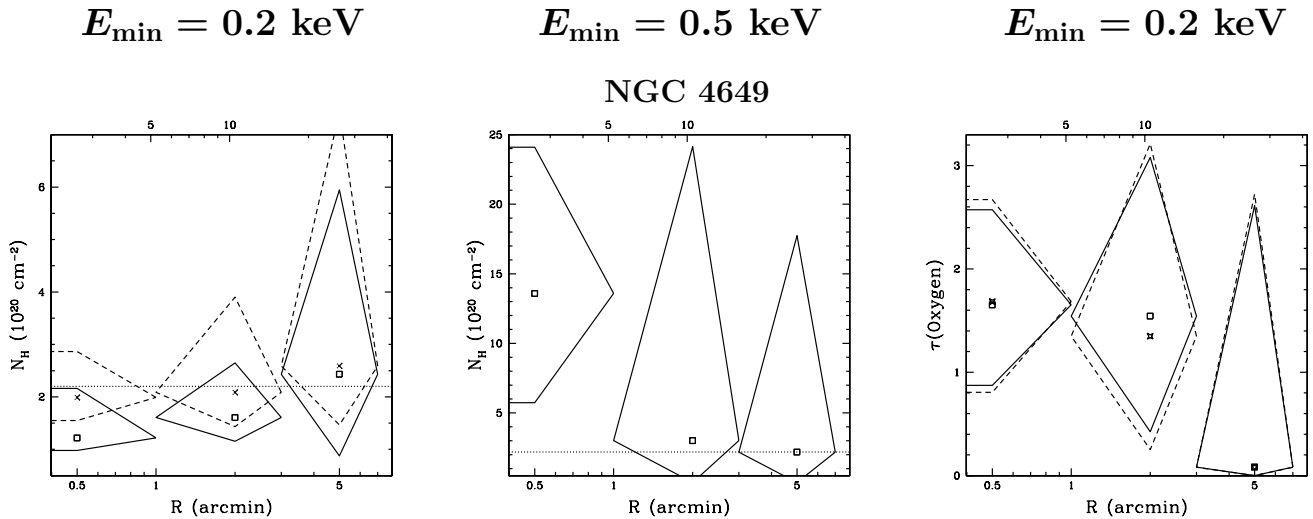


FIG. 4.— As Figure 1 but for the one system with 3 annuli.

TABLE 1
QUALITY OF FITS AND EDGE OPTICAL DEPTH FOR $r = 1'$

Name	N_{H}	No Edge			Edge			τ	F Test $P(F)$
		χ^2	dof	P	χ^2	dof	P		
N507	Fix	36.2	47	0.87	32.2	46	0.94	1.9(0.59)	2.7E-2
	Free	34.0	46	0.91	30.4	45	0.95	1.5(0.49)	2.6E-2
N533	Fix	29.9	31	0.52	29.7	30	0.48	0.55(0.00)	0.66
	Free	28.9	30	0.52	28.9	29	0.47	0.00(0.00)	1.00
N1399	Fix	106.9	97	0.23	83.7	96	0.81	3.8(0.89)	1.3E-6
	Free	104.9	96	0.25	83.7	95	0.79	3.3(0.97)	3.9E-6
N2563	Fix	24.0	25	0.52	22.9	24	0.53	1.5(0.00)	0.29
	Free	23.6	24	0.48	22.9	23	0.47	1.3(0.00)	0.41
N4472	Fix	209.0	104	4.7E-9	158.1	103	4.0E-4	1.5(0.74)	8.8E-8
	Free	158.9	103	3.4E-4	142.2	102	5.3E-3	1.3(0.25)	7.9E-4
N4636	Fix	109.9	52	4.9E-6	105.8	51	1.0E-5	1.3(0.00)	0.17
	Free	104.7	51	1.4E-5	103.1	50	1.5E-5	0.58(0.00)	0.38
N4649	Fix	67.2	61	0.27	58.1	60	0.55	1.7(0.44)	3.2E-3
	Free	63.4	60	0.36	57.8	59	0.52	1.7(0.00)	2.0E-2
N5044	Fix	191.2	118	2.3E-5	156.5	117	8.7E-3	1.8(0.59)	9.2E-10
	Free	138.6	117	8.5E-2	126.4	116	0.24	1.3(0.45)	1.1E-3
N5846	Fix	84.0	47	7.4E-4	78.4	46	2.1E-3	0.83(0.00)	7.6E-2
	Free	74.6	46	4.8E-3	72.6	45	5.7E-3	0.57(0.00)	0.27
H62	Fix	37.8	46	0.80	37.7	54	0.77	0.16(0.00)	0.73
	Free	38.6	45	0.74	37.7	44	0.74	0.46(0.00)	0.31

NOTE.—Results of deprojection analysis in the central radial bin ($R = 1'$). Models where the column density of the standard foreground absorber with solar abundances is fixed to the Galactic value are indicated by “Fix” under the N_{H} column; variable column models are indicated by “Free”. For the models with an intrinsic oxygen edge at 0.532 keV (rest frame) we list the best-fitting optical depth, τ , with its 95% confidence lower limit in parentheses. The χ^2 null hypothesis probability is listed in the column P under the assumption of gaussian random errors (see section 3.4 of PAPER2). The F-Test probability, $P(F)$ (e.g., Bevington 1969), quantifies the improvement in χ^2 when adding the edge; i.e., $P(F) \ll 1$ indicates significant improvement.

the values of ΔN_{H} quoted do refer to quantities within the 3D radius $r = 1'$.)

Entirely analogous results are obtained for the other systems in our sample. We mention that partial covering models never improve the fits over the $f = 1$ case. The only effect is that somewhat larger columns are generally allowed; e.g., for $f = 0.5$ the implied upper limits for the excess columns are typically a factor of 20%-40% larger than for $f = 1$.

Hence, as in PAPER1 we conclude that models with $f < 1$ cannot account for (1) the large excess columns inferred from ASCA, (2) the sub-Galactic columns and poor

fits obtained for several systems in the central $1'$, or as we now discuss (3) the sensitivity of N_{H} to the lower energy boundary of the bandpass.

3.3. Sensitivity of $N_{\text{H}}(R)$ to Bandpass

Thus far we have shown (and confirmed previous results) that the ROSAT PSPC does not indicate the presence of excess absorbing material arising from cold gas intrinsic to the galaxy or group. In Figure 5 (Left) we display the ROSAT PSPC spectrum of NGC 1399 within the central arcminute along with the best-fitting plasma model modified by a standard absorber with $N_{\text{H}} = N_{\text{H}}^{\text{Gal}}$. The simple

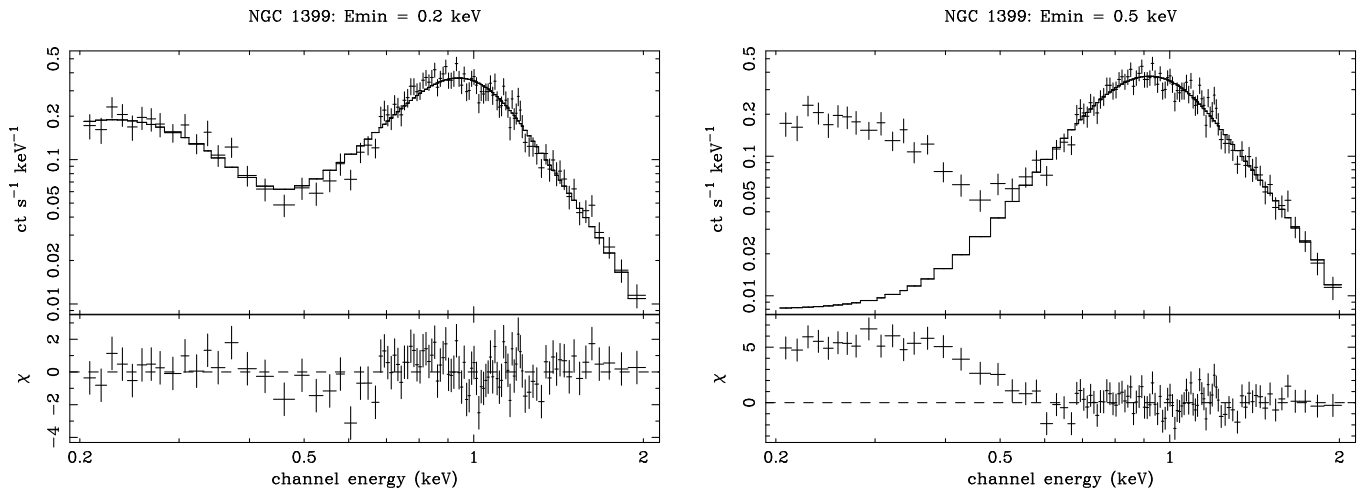


FIG. 5.— (Left) *ROSAT* PSPC spectrum within $R = 1'$ of NGC 1399. Also shown is the best-fitting single-phase plasma model modified by the standard absorber with $N_{\text{H}} = N_{\text{H}}^{\text{Gal}}$. (Right) The best fitting model with variable N_{H} when only energies above 0.5 keV are included in the fit. In this case the fitted column density is $N_{\text{H}} \sim 15N_{\text{H}}^{\text{Gal}}$; i.e., when $E_{\text{min}} = 0.5$ keV the standard absorber model predicts that there should be negligible emission at lower energies in conflict with the observation.

model provides a good visual fit to these data as well as a formally acceptable fit ($\chi^2 = 107$ for 97 dof and $P = 0.23$).

However, the evidence for intrinsic soft X-ray absorption from cold gas in galaxies, groups, and clusters from the *Einstein* SSS and the *ASCA* SIS is obtained with data restricted to energies above ~ 0.5 keV because lower energies reside outside the bandpasses of those instruments. Let us examine what happens to the spectral fits of the PSPC data of NGC 1399 within the central arcminute if instead we raise the lower energy limit of the bandpass, E_{min} , to a value near 0.5 keV comparable to *ASCA* and *Einstein*, and we allow N_{H} to be a free parameter.

We find that when $E_{\text{min}} \approx 0.2\text{--}0.3$ keV we obtain fits essentially as indicated in Figure 5 (Left) with $N_{\text{H}} \approx N_{\text{H}}^{\text{Gal}}$. We see a noticeable change near $E_{\text{min}} = 0.4$ keV when the fitted column density increases to $N_{\text{H}} \approx 2N_{\text{H}}^{\text{Gal}}$. A dramatic increase occurs near $E_{\text{min}} = 0.5$ keV which we show in Figure 5 (Right). The best-fitting model gives $N_{\text{H}} \approx 15N_{\text{H}}^{\text{Gal}}$ when data below 0.5 keV are excluded from the fits: the standard absorber model when $E_{\text{min}} = 0.5$ keV predicts that there should be negligible emission at lower energies in clear conflict with the data for $E \sim 0.2\text{--}0.3$ keV. The large column density obtained when $E_{\text{min}} = 0.5$ keV is similar to the large value inferred from *ASCA* with two-temperature or cooling flow models (see §5 in Buote 1999).

For larger values of E_{min} we find that N_{H} does not change significantly within the uncertainties. The statistical uncertainties on the fitted spectral parameters increase with increasing E_{min} since the degrees of freedom decrease as the lower energy data are ignored.

In the middle panels of Figures 1-4 we plot $N_{\text{H}}(R)$ for $E_{\text{min}} = 0.5$ keV. The character of the N_{H} profiles for $E_{\text{min}} = 0.5$ keV is entirely different from the previous $E_{\text{min}} = 0.2$ keV case for half of the sample: NGC 507, 1399, 4472, 4649, and 5044. In these systems $N_{\text{H}}(R)$ for $E_{\text{min}} = 0.5$ is consistent with the Galactic values in the outermost annuli and *increases* as R decreases until (except for NGC 4472) it reaches a value consistent with a maximum for $R \sim 1'$. For the other five galaxies the con-

straints are too poor to discern a trend, though within the large errors their profiles are consistent with increasing as $R \rightarrow 0$.

The excess column densities inferred when $E_{\text{min}} = 0.5$ keV are most significant for NGC 1399. The lower limits within $R = 1'$ are $8 \times 10^{20} \text{ cm}^{-2}$ and $3 \times 10^{20} \text{ cm}^{-2}$ at 95% and 99% confidence respectively which are factors of ≈ 6 and 3 larger than the Galactic value. Also within $R = 1'$ for NGC 507 we obtain 95%/99% lower limits of $8/6 \times 10^{20} \text{ cm}^{-2}$ compared to the adopted Galactic value of $5.2 \times 10^{20} \text{ cm}^{-2}$. The most significant measurement for NGC 5044 is within the $R = 1' - 2'$ annulus where we find that $N_{\text{H}} > N_{\text{H}}^{\text{Gal}}$ at the 95% confidence level.

In order to obtain measurements of the intrinsic absorption at a higher significance level we must include the data below 0.5 keV. This requires a more appropriate model of the intrinsic absorption that does not conflict with the emission at lower energies which we now consider.

3.4. Intrinsic Oxygen Edge

Since we find that $N_{\text{H}}(E_{\text{min}}) \approx \text{constant}$ for $E_{\text{min}} \gtrsim 0.5$ keV, the portion of the spectrum responsible for the excess absorption must be near 0.5 keV. Considering the PSPC resolution $[\Delta E/E = 0.43(E/0.93\text{keV})^{-0.5}]$ and effective area this translates to energies $\sim 0.4\text{--}0.7$ keV. The dominant spectral features in both absorption and emission over this energy range are due to oxygen, though ionized carbon and nitrogen can contribute as well (see §5.2).

Since the PSPC data cannot distinguish between a single edge and multiple edges, we parameterize the intrinsic absorption with a single absorption edge at 0.532 keV (rest frame) corresponding to cold atomic oxygen (O I). In the right columns of Figures 1-4 we plot the optical depth profiles, $\tau(R)$, for the O I edge obtained from fits with $E_{\text{min}} = 0.2$ keV.

For every system we find that the shape of $\tau(R)$ is very similar to that of $N_{\text{H}}(R)$ for $E_{\text{min}} = 0.5$ for the standard absorber. Moreover, for those systems where $N_{\text{H}} \gg N_{\text{H}}^{\text{Gal}}$ for $E_{\text{min}} = 0.5$ we find that $\tau(R) \lesssim 0.1$ in the outermost annuli and increases to $\tau(R) \sim 1$ in the central bin.

Therefore, the single oxygen edge reproduces all of the excess absorption indicated by $N_{\text{H}}(R)$ for $E_{\text{min}} = 0.5$ for the standard absorber model.

The fits within the central radial bin are clearly improved for several systems when the single oxygen edge is added, even though in some cases the quality of the fit is already judged to be formally acceptable (null hypothesis $P \gtrsim 0.1$) without the edge. The improvement in the χ^2 fit is quantified by the F Test (e.g., Bevington 1969), and in Table 1 for each galaxy and group we give the F-Test probability, $P(F)$, which compares the fits with and without the edge; i.e., $P(F) \ll 1$ indicates the edge improves the fit significantly.

Concentrating on models with the standard absorber with $N_{\text{H}} = N_{\text{H}}^{\text{Gal}}$ we see in Table 1 the largest improvements exist for NGC 5044 ($P(F) = 9.2 \times 10^{-10}$), NGC 4472 ($P(F) = 8.8 \times 10^{-8}$), and NGC 1399 ($P(F) = 1.3 \times 10^{-6}$). A very significant improvement is also found for NGC 4649 ($P(F) = 3.2 \times 10^{-3}$) while marginal improvements are found for NGC 507 ($P(F) = 2.7 \times 10^{-2}$) and NGC 5846 ($P(F) = 7.6 \times 10^{-2}$). Although only NGC 4472, 5044, and 5846 are indicated to have formally unacceptable fits in terms of the χ^2 null hypothesis probability for models with or without the edge, the fact that adding the edge lowers χ^2 by much more than 1 (i.e., $P(F) \ll 1$) in several cases indicates that the fits are indeed better with the edge in those systems.

For every system where we found $N_{\text{H}} < N_{\text{H}}^{\text{Gal}}$ for the standard absorber (§3.1), we find that N_{H} systematically increases when the oxygen edge is added. Although the addition of the edge results in $N_{\text{H}} \sim N_{\text{H}}^{\text{Gal}}$ for many of these systems we find that in some cases (most notably NGC 5044) N_{H} is still significantly less than $N_{\text{H}}^{\text{Gal}}$, and the fits in the central bin, though improved, are still formally unacceptable. Thus, adding the edge does significantly improve the models, but it apparently is not the only improvement required in some cases. We discuss another mechanism to improve the fits below in §3.6.3.

We obtain the best constraints on the edge optical depth for NGC 507, 1399, 4472, 4649, and 5044. Only for these systems is $\tau > 0$ significant at the 95% confidence level in the central bin whether or not N_{H} is fixed to the Galactic value for the standard absorber model. In some cases $\tau > 0$ is significant at the 99% level – we discuss individual cases below in §3.5.

We have also investigated whether these oxygen absorption profiles can be reproduced by a profile of decreasing oxygen abundance; i.e., the strong $K\alpha$ lines of O VII and O VIII lie between 0.5-0.65 keV. If instead we allow the oxygen abundance in the hot gas to be a free parameter in the fits we find that typically the best-fitting oxygen abundance is zero, and the quality of most of the fits are improved similarly to that found when the oxygen edge is added. This degeneracy is not surprising owing to the limited energy resolution of the PSPC. The notable exception is NGC 1399 where the fits for $r = 1'$ are only improved to $\chi^2 = 95.9$ for zero oxygen abundance as opposed to 83.7 for the edge (both have variable N_{H}). However, zero oxygen abundance in the centers is highly unlikely because of the expected enrichment from the stars in the central galaxy. And if instead we consider plausible O/Fe ratios to be at least 1/2 solar in NGC 507, 1399, 4472, 4649,

and 5044, then the fits are not as much improved as when adding the edge.

As mentioned above (and in PAPER1) we find that for most radii the constraints on the edge energy are not very precise which is why we fixed the edge energy in our analysis. The best constraints are available for NGC 1399 and 5044 within the central bin for which we obtain $0.51^{+0.05}_{-0.05}$ keV and $0.51^{+0.09}_{-0.05}$ keV (90% confidence) for the edge energies for the standard absorber models with variable N_{H} . (Models with fixed foreground Galactic columns give similar results; e.g., $0.53^{+0.05}_{-0.03}$ keV for NGC 1399.)

These constraints are consistent with the lower ionization states of oxygen but not edges from the highest states O VI-VIII. Due to the limited resolution we can add additional edges to “share” the τ obtained for the O I edges, although when using a two-edge model a significant τ cannot be obtained for edge energies above ~ 0.65 keV corresponding to \sim O VI.

3.5. Comments on Individual Systems

We elaborate further on the results for individual systems. When comparing N_{H} profiles to those obtained from previous ROSAT PSPC studies we implicitly account for any differences in the plasma codes and solar abundances used.

3.5.1. Systems with 7 Annuli

In Figure 1 we display the results for the three systems where the spectral parameters are well determined in seven annuli. These observations thus generally correspond to the highest S/N data in our sample. The evidence for intrinsic oxygen absorption is strongest for these systems.

NGC 507: The oxygen edge optical depth, $\tau(R)$, falls gradually from the center and remains significantly non-zero out to $R \sim 4'$; e.g., in the $R = 3'-4.25'$ annulus the 95% confidence lower limits on τ are 0.39 and 0.24 respectively in models with fixed (Galactic) and variable N_{H} for the standard absorber. The values of N_{H} for the standard absorber are consistent with those obtained by Kim & Fabbiano (1995) with the PSPC data.

NGC 1399: This system exhibits the most centrally peaked τ profile in our sample. Within the central arcminute $\tau > 0.26$ and 0.33 at 99% confidence respectively for the fixed and free N_{H} models. At larger radii the non-zero optical depths are also quite significant; e.g., for $R = 2.5'-4'$ $\tau > 0.64$ and 0.50 at 99% confidence for the fixed and free N_{H} models. We obtain values of N_{H} for the standard absorber consistent with the previous PSPC study by Jones et al (1997).

NGC 5044: The second radial bin ($R = 1'-2'$) actually has a smaller uncertainty on the oxygen edge optical depth than the central bin; i.e., the 95% lower limits on τ are 0.87 and 0.79 respectively for the fixed and free N_{H} models. In fact, the corresponding 99% lower limits are 0.75 and 0.42 for $R = 1'-2'$ which are larger than the values for the $R = 1'$ bin. The optical depth remains significantly non-zero out to the $R = 3'-4.5'$ bin in which we obtain 95% lower limits on τ of 0.36 and 0.10 for the fixed and free N_{H} models. Our values of N_{H} are consistent with those obtained from the PSPC data by David et al (1994).

3.5.2. Systems with 5-6 Annuli

In Figure 2 we display the results for the three systems where the spectral parameters are well determined in 5-6 annuli. Only for NGC 4472 is the intrinsic oxygen absorption clearly significant.

NGC 2563: The uncertainties on $\tau(R)$ are large and consistent with zero at the center. However, the shapes of the error regions, especially the large uncertainty at the center, are consistent with the same type of increasing τ profile with decreasing R found for the systems with seven annuli.

NGC 4472: The optical depth is consistent with $\tau \sim 2$ for $R \lesssim 5'$ and then decreases rapidly at larger radii. Unlike the other systems with evidence for intrinsic absorption τ is most significant away from the central bin; i.e., for $R = 3.25' - 5'$ the 95% confidence lower limits on τ are 1.62 and 1.75 respectively for the fixed and free N_{H} models. (The corresponding 99% lower limits are 1.27 and 1.46.) Interestingly, $R \sim 5'$ corresponds to the region where Irwin & Sarazin (1996) identified holes in the X-ray emission from visual examination of the PSPC image, and thus the large oxygen edge optical depths could be related to these holes. The sub-Galactic columns obtained for the standard absorber with variable N_{H} are consistent with those obtained by Forman et al (1993).

NGC 5846: The uncertainties on $\tau(R)$ are large, and although a substantial amount of intrinsic absorption is allowed by the data, no excess absorption is required.

3.5.3. Systems with 4 Annuli

In Figure 3 we display the results for the three systems where the spectral parameters are well determined in 4 annuli. The uncertainties on $\tau(R)$ are large for each of these systems and thus no intrinsic oxygen absorption is clearly required by the data.

3.5.4. Systems with 3 Annuli

In Figure 4 we display the results for the one system where the spectral parameters are well determined in only 3 annuli, NGC 4649. In contrast to the systems with 4 annuli we find evidence for significant intrinsic oxygen absorption in the central bin for NGC 4649.

NGC 4649: In the central radial bin the 90% lower limits on τ are 0.55 and 0.20 respectively for the fixed and free N_{H} models, although only the 95% lower limit for the model with fixed N_{H} is significantly larger than zero (Table 1). Our values of N_{H} for the standard absorber are consistent with those obtained from the PSPC data by Trinchieri et al (1997).

3.6. Multiphase Models

3.6.1. Simple Cooling Flow

In the inhomogeneous cooling flow scenario the hot gas is expected to emit over a continuous range of temperatures in regions where the cooling time is less than the age of the system. We consider a simple model of a cooling flow where the hot gas cools at constant pressure from some upper temperature, T_{max} (e.g., Johnstone et al 1992). The differential emission measure of the cooling gas is proportional to $\dot{M}/\Lambda(T)$, where \dot{M} is the mass deposition rate of gas cooling out of the flow, and $\Lambda(T)$ is the cooling function of the gas (in our case, the MEKAL plasma code).

Since the gas is assumed to be cooling from some upper temperature T_{max} , the cooling flow model requires that there be a reservoir of hot gas emitting at temperature T_{max} but is not cooling out of the flow. Consequently, our cooling flow model actually consists of two components, CF+1T, where ‘‘CF’’ is the emission from the cooling gas and ‘‘1T’’ is emission from the hot ambient gas. We set T_{max} of the CF component equal to the temperature of the 1T component, and both components are modified by the same photoelectric absorption. This simple model of a cooling flow is appropriate for the low energy resolution of the ROSAT PSPC and has the advantage of being well studied, relatively easy to compute, and a good fit to the ASCA data of many elliptical galaxies and groups (e.g., Buote & Fabian 1998; Buote 1999, 2000a).

When fitting this cooling flow model to the ROSAT spectra of the galaxies and groups in our sample we find that if only absorption from the standard cold absorber model with solar abundances is included then we obtain results identical to the single-phase models; i.e., the CF component is clearly suppressed by the fits. Since the CF model includes temperature components below ~ 0.5 keV it has stronger O VII and O VIII lines than the single-phase models which, as shown above, already predict too much emission from these lines. It is thus not surprising that only when an intrinsic oxygen absorption edge is included in the fits can we obtain a significant contribution from a CF component.

Even when adding the oxygen edge the cooling flow models do not improve the fits perceptively in any case. And since the magnitude of τ for the oxygen edge is degenerate with \dot{M} of the cooling flow component, the constraints on both parameters are quite uncertain. For NGC 5044, which has the best constraints, adding the CF component improves χ^2 from 156.5 to 154.1 for 116 dof within the central arcminute (i.e., marginal improvement). The oxygen edge optical depths are consistent with those obtained from the single-phase analysis. Only within $r = 2'$ is there an indication of significant cooling with $\dot{M} \sim 12M_{\odot}\text{yr}^{-1}$ which is very consistent with the ROSAT results of David et al (1994) within the same radius. (Our mass deposition rates have large statistical uncertainties because of the inclusion of the intrinsic oxygen edge.)

Thus, simple cooling flow models give results that are entirely consistent with the single-phase models.

3.6.2. Two Hot Phases

A two-temperature model (2T) is a more flexible multiphase emission model than the constant-pressure cooling flow and can very accurately mimic a cooling flow spectrum over typical X-ray energies (Buote, Canizares, & Fabian 1999). If we restrict the temperatures of the 2T model to lie between $\sim 0.5 - 2$ keV appropriate for hot gas near the virial temperatures of these galaxies and groups, then we obtain results equivalent to the cooling flow models above; e.g., (1) the extra temperature component is only allowed if the intrinsic oxygen edge included, and (2) results are entirely consistent with the single-phase models. Since the temperatures of the 2T models are fitted separately, constraints on the 2T models are even poorer than the cooling flows because of the extra free parameter.

3.6.3. Two-Phase Medium: Warm and Hot Gas

Recall that when fitted with only a standard absorber with solar abundances that $N_{\text{H}}(R)$ decreases as R decreases such that N_{H} is less than $N_{\text{H}}^{\text{Gal}}$ near $R = 0$ for most of the galaxies and groups (§3.1). This trend implies the existence of excess soft X-ray emission above that produced by the hot gas, the signature of which is most evident at the centers of these galaxies and groups. Although the sub-Galactic values of N_{H} are only marginally significant in many cases, they are highly significant for NGC 4472 and NGC 5044.

If the excess soft X-rays near the centers represent emission from coronal gas, then the temperatures must be $\lesssim 0.1$ keV (i.e., distinctly cooler than the hot gas phase). For NGC 5044, which has the most significant sub-Galactic column densities in the central bins, we find that when adding an extra temperature component to the single-phase model modified only by the standard absorber with $N_{\text{H}} = N_{\text{H}}^{\text{Gal}}$ (i.e., no intrinsic oxygen edge), that the fits are improved very similarly to the single-phase models when N_{H} is allowed to take a value significantly less than $N_{\text{H}}^{\text{Gal}}$. For example, in the central bin the fit improves from $\chi^2 = 191$ (118 dof) for the 1T model to $\chi^2 = 133$ (116 dof) for the 2T model (both models with $N_{\text{H}} = N_{\text{H}}^{\text{Gal}}$) very similar to the result obtained for the 1T model with $N_{\text{H}} < N_{\text{H}}^{\text{Gal}}$ (i.e., $\chi^2 = 139$ for 117 dof – “Free” in Table 1). Essentially the same large improvement is found for the second radial bin ($R = 1' - 2'$). Significant but smaller improvement in the fits ($\Delta\chi^2 \sim 10$) is also seen in the third and fourth bins (i.e. $R = 2' - 4.5'$).

The inferred temperature of the soft component in the central bin is $T = 0.05_{-0.03}^{+0.03}$ keV ($6_{-4}^{+4} \times 10^5$ K) at 90% confidence consistent with values obtained for other radii; i.e., consistent with “warm” gas rather than “hot” gas near the virial temperatures of the galaxies and groups. Gas at these warm temperatures is not optically thin to photons with energies near 0.5 keV (e.g., Krolik & Kallman 1984), and thus this warm gas may be responsible for the intrinsic oxygen absorption inferred in §3.4. However, since this warm gas is apparently partially photoionized by the hot gas (and perhaps by itself) a proper calculation of the emission from the warm gas must consider radiative transfer effects which is beyond the scope of this paper. (We shall continue to use the optically thin models in this paper.) We discuss the properties of this warm gas in more detail in §5.

The improvement obtained in the fit when adding a component of warm gas to the single-phase model ($N_{\text{H}} = N_{\text{H}}^{\text{Gal}}$) is somewhat larger than that obtained when adding the single oxygen edge (i.e., $\chi^2 = 133$ for 116 dof for the 2T model versus $\chi^2 = 156.5$ for 117 dof for the edge – Table 1). Unfortunately, due to the limited energy resolution of the PSPC it is very difficult to obtain simultaneous constraints on both absorption and emission models for both the warm and hot gas.

The most reliable constraints on the warm gas component are possible for NGC 5044 because for 1T models we find that N_{H} of the standard absorber is well below $N_{\text{H}}^{\text{Gal}}$ at small R whether or not an intrinsic oxygen edge is included (Figure 1). For a 2T model with an intrinsic oxygen edge we find that the temperature of the warm component

in the central bin is $T = 0.06_{-0.04}^{+0.03}$ keV ($7_{-5}^{+4} \times 10^5$ K) at 90% confidence consistent with that obtained for the 2T model without the oxygen edge. The oxygen edge optical depth is not very well constrained, $\tau = 0.8_{-0.6}^{+0.4}$, $1.2_{-0.7}^{+0.8}$ (90% confidence) in the inner two bins respectively, which is about half the best-fitting value and near the 95% lower limit of τ obtained without including the emission from the warm gas (Table 1). The weakened constraint on the oxygen edge optical depth for the 2T model of NGC 5044 reflects the relatively small improvement in the fit (χ^2 of 127 for 115 dof) over the 2T model without an edge. For the other galaxies, most notably NGC 1399, the constraints on the oxygen edge are not weakened nearly as much.

Emission from such a warm gas component is consistent with, though not as clearly required by, the PSPC data for the other systems. Only for NGC 4472 is clearly significant improvement found when adding both the warm gas component and the oxygen edge. Temperatures ($T \sim (5 - 10) \times 10^5$ K) and the reduction in edge optical depth are obtained similarly as found for NGC 5044. Future observations with better energy resolution are required to definitively confirm and measure the emission and absorption properties of the warm gas in all of these systems.

3.7. Caveats

(i) *Calibration:* The gain of the PSPC is well calibrated and in particular no significant calibration problems near 0.5 keV have been reported.³ The large values of $\tau \sim 1$ obtained in the central regions imply that the absorption significantly affects a large energy range comparable to the energy resolution of the PSPC; e.g., the O I edge absorbs 25% of the flux at 0.8 keV for $\tau = 1$; i.e. possible residual calibration errors near 0.5 keV where the effective area is changing rapidly (e.g., Figure 1 of Snowden et al 1994) can not explain the need for absorption at higher energies. Moreover, the shape of $\tau(R)$ is not the same for each system as would be expected if calibration were responsible for the intrinsic oxygen absorption found in half of the sample; e.g., $\tau(R)$ for NGC 1399 is much more centrally peaked than for NGC 4472 or the other systems. The agreement between the absorption inferred by the PSPC and ASCA mentioned below in §4 further argues against a systematic error intrinsic to the PSPC being responsible for the measured oxygen absorption.

(ii) *Galactic Columns:* All of the objects in our sample reside at high Galactic latitude, and thus the Galactic absorption should be fairly uniform over the relevant 5'-10' scales. Errors in the assumed Galactic columns (Dickey & Lockman, 1990) should only affect the baseline value and not the variation with radius.

(iii) *Background:* Errors in the background level affect most seriously the lowest energies ($\lesssim 0.4$ keV) which are also most sensitive to the column density of the standard absorber model. Hence, measurements of N_{H} at the largest radii (which have lowest S/N) are the most affected by background errors. The hydrogen column densities measured in the outer radii (see Figures 1-4) are very similar to and are usually consistent with the assumed Galactic values within the estimated 1σ errors which attests to the accuracy of our background estimates. The intrinsic oxygen optical depths in the central radial bins

³See <http://heasarc.gsfc.nasa.gov/docs/rosat>.

are very insensitive to the background level.

4. COMPARISON TO ASCA

The intrinsic oxygen absorption indicated by the PSPC data in half of our sample is most significant within the central $1' - 2'$ which is similar to the width of the ASCA PSF. In addition, since the ASCA SIS is limited to $E > 0.5$ keV, and the efficiency near 0.5 keV is severely limited due to instrumental oxygen absorption, it cannot be expected that ASCA can distinguish an oxygen edge from a standard absorber with solar abundances. However, it is instructive to examine the consistency between results obtained from spatially resolved (PSPC) and single-aperture (ASCA) methods. As mentioned in PAPER1 the results obtained when adding an oxygen edge to the ASCA data of NGC 1399 and 5044 are consistent with those obtained with the PSPC. Since similar results are found for other objects in our sample showing intrinsic absorption, we focus on NGC 1399 for illustration.

Previously we (Buote, 1999) have fitted two-temperature models to the accumulated ASCA SIS and GIS data within $R \approx 5'$ of NGC 1399 and obtained $N_{\text{H}}^{\text{c}} = 49_{-9}^{+6} \times 10^{20} \text{ cm}^{-2}$ (90% confidence) for the standard absorber on the cooler temperature component. Using the meteoritic solar abundances (see §4.1.3 of PAPER2) slightly modifies this result to $N_{\text{H}}^{\text{c}} = 40_{-7}^{+6} \times 10^{20} \text{ cm}^{-2}$ which is about 30 times larger than the Galactic value ($N_{\text{H}}^{\text{c}} = 1.3 \times 10^{20} \text{ cm}^{-2}$). Comparing this result to those obtained from the PSPC for $E_{\text{min}} = 0.5$ keV (Fig 1) we see that the ASCA column density is qualitatively similar to the value of $N_{\text{H}} \approx 20 \times 10^{20}$ obtained within $R = 1'$ and is consistent with the total column within $R \approx 5'$. If instead the columns of the standard absorber are fixed to Galactic on both components, and an intrinsic O I edge is added to the cooler component, then we obtain $\tau = 6.0_{-0.7}^{+0.7}$ (90% confidence) for the ASCA data. Again this ASCA result is similar to $\tau \sim 4$ in the central PSPC bin and is very consistent with the value of $\tau = 5.7$ obtained from adding up the best-fitting values obtained with the PSPC within $R = 5'$. Therefore, the oxygen edge provides as good or better description of the excess absorption inferred from multitemperature models of ASCA data within the central few arcminutes as a standard cold absorber with solar abundances, and yields optical depths that are consistent with those obtained with the PSPC data.

Although a similar consistency is achieved for NGC 4472 the interpretation of the absorption of the two-component model of the single-aperture ASCA data is not so straightforward because the absorption is not obviously concentrated at the center (i.e. on the cooler temperature component). In fact, a spatially uniform absorber within $R = 5'$ is probably a better description of the PSPC data. If the column densities on both temperature components are tied together for the two-temperature model of the ASCA data the quality of the fit is slightly worse ($\Delta\chi^2 = 8$ for 361 dof), but $N_{\text{H}} \approx 11 \times 10^{20} \text{ cm}^{-2}$ which is a fair representation of the average N_{H} profile obtained from the PSPC for $E_{\text{min}} = 0.5$ keV (Fig 2). Similar agreement is found for the O I edge when applied to both temperature components.

5. WARM IONIZED GAS IN COOLING FLOWS

We consider now in some detail the properties of the intrinsic absorber and their implications. Initially we focus our attention on the physical state of the absorber.

5.1. Why Not Dust?

Models of dust grains indicate that dust can give rise to significant amounts of absorption between 0.1-1 keV (e.g., Laor & Draine 1993). In principle such grains could explain the intrinsic absorption we have inferred for energies above ~ 0.5 keV in the PSPC data of half of the galaxies and groups in our study as well as the excess absorption detected for energies above ~ 0.5 keV in the ASCA data of bright galaxies, groups, and clusters.

However, dust should also heavily absorb X-rays with energies between 0.1 – 0.4 keV (e.g., Laor & Draine 1993) which is inconsistent with the ROSAT data for the 10 galaxies and groups in our study and, e.g., the large sample of ROSAT clusters studied by Allen & Fabian (1997). To evade this constraint (i.e., no absorption below 0.4 keV) an unconventional model for the formation of dust grains has to be postulated; e.g., dust grains condense out of a medium in which helium remains ionized (Arnaud & Mushotzky, 1998). Even if we consider the (rather unlikely) possibility that dust does not absorb X-rays below ~ 0.4 keV, we still have that dust cannot account for the excess X-ray emission at those energies implied by the sub-Galactic column densities (§3.1 and 3.6.3).

Other strong arguments against the existence of large quantities of oxygen-absorbing dust in cooling flows have been made in the past. At the centers of cooling flows where the gas density is largest and the soft X-ray absorption is most significant dust should not be present in large quantities because the grains are rapidly destroyed by sputtering by the hot gas (e.g., Tsai & Mathews 1995; Voit & Donahue 1995). A different argument due to Voit & Donahue (1995) considers that the transient heating of the grains by X-rays from the hot gas prevents CO from fully condensing onto dust grains. Consequently, significant amounts of oxygen would remain in molecular gas which would produce CO emission from rotational lines that are inconsistent with the generally negligible CO detections in cooling flows (e.g., Bregman, Hogg, & Roberts 1992; O'Dea et al 1994).

5.2. Temperature of the Warm Ionized Gas

Unlike dust all of the key features of the observed soft X-ray absorption and emission can be accounted for if the absorber is (primarily) collisionally ionized gas. The lack of intrinsic absorption observed for energies between $\sim 0.2 - 0.4$ keV in the ROSAT data requires that H and He be completely ionized implying a gas temperature $T \gtrsim 1.0 \times 10^5$ K (e.g., Sutherland & Dopita 1993). In order to have significant absorption at 0.5 keV the temperature cannot be larger than $\approx 1 \times 10^6$ K (see Figure 2 of Krolik & Kallman 1984). This *absorbing* temperature range ($T = 10^{5-6}$ K) is entirely consistent with that inferred from the gas *emission* to explain the sub-Galactic column densities especially for NGC 5044 (§3.6.3). This consistency of absorption and emission properties lends strong support to the idea that the absorber is warm ionized gas.

At these temperatures carbon and nitrogen are not completely ionized (e.g., Nahar & Pradhan 1997; Sutherland

& Dopita 1993), and thus these elements will also contribute to the soft X-ray absorption. For nitrogen the states N_{IV-VI} are significant, and their edge energies span 0.46-0.55 keV (rest frame) which are consistent with the edge energy range determined from the PSPC data. Since $N/O = 1/8.51$ (assuming solar abundance ratios), and the threshold cross sections for absorption are similar for N and O, only $\sim 12\%$ of the optical depth we have measured in each system likely arises from ionized nitrogen.

The ionization fraction for carbon changes rapidly near $T = 10^5$ K with C_V dominating for temperatures above this value and up to $T \approx 10^6$ K. The edge energy for C_V is 0.39 keV, and since $C/O \approx 0.5$ (assuming solar abundance ratios) and the threshold cross sections of C and O are similar, the optical depth of C_V is about half that expected from a dominant ionized state of oxygen. However, the strong instrumental carbon absorption leaves the PSPC with essentially no effective area over energies 0.28 keV to ~ 0.4 keV (e.g., see Figure 1 of Snowden et al 1994), and thus it is only possible to detect intrinsic absorption from the C_V edge for energies above ~ 0.4 keV even considering the smearing due to the limited energy resolution. This is entirely consistent with the variation of N_H with E_{min} described in §3.3.

Considering the energy resolution and effective area curve of the PSPC, the 0.532 keV edge that we have used to parameterize the intrinsic absorption is likely an average of the $\sim 40\%$ contribution from the C_V edge (0.39 keV) and N_{IV-VI} edges (0.46-0.55 keV) with a $\sim 60\%$ contribution from ionized oxygen states. Although as discussed in §3.4 the PSPC data cannot distinguish between multi-edge models, when using a more realistic absorber model consisting of C_V and N_{VI} and an oxygen edge, we are able to obtain a significant optical depth for the oxygen edge for energies as high as ~ 0.75 keV consistent with O_{VII} (0.74 keV). However, to insure that oxygen produces at least as much absorption as the C and N edges, the PSPC data also require a contribution from edges around $\sim 0.6 - 0.65$ keV corresponding to edges from O_{IV-VI} .

Consideration of these maximum allowed ionization states for oxygen indicates that the maximum temperature of the warm gas is more like $T \approx 5 \times 10^5$ K if the gas is isothermal and collisionally ionized (e.g., Nahar 1999; Sutherland & Dopita 1993). The absorption signature of this warm gas is not one dominant feature near 0.5 keV but is rather a relatively broad trough over energies 0.4 to ~ 0.8 keV for total optical depths of unity (see Figure 1 of Krolik & Kallman 1984).

(We mention that the edge energies we have quoted are from Daltabuit & Cox (1972) though Gould & Jung (1991) argue that the edge energy for O_I is ~ 10 eV higher. Such differences may be relevant for modeling future high resolution spectra but are unimportant for our present discussion with the PSPC data.)

Hence, a proper absorber model needs to consider several edges from different ionization states of oxygen as well as edges from ions of C and N. Since the warm gas absorbs photons from the hot gas the assumption of collisional ionization equilibrium is also not strictly valid nor is it clear that the warm gas is fully optically thin to its own radiation as was assumed in §3.6.3 for convenience. Consequently, the single-edge oxygen absorber that we have used throughout this paper (and PAPER1) has been in-

tended primarily as a phenomenological tool to establish the existence and to study the gross properties of the absorber which is appropriate for the low spectral resolution afforded by the PSPC data. If our basic results are confirmed with the substantially higher quality data from *Chandra* and *XMM*, then it will be appropriate to expend the effort to construct rigorous models of the warm absorber accounting for many edges and possible radiative transfer effects that are not currently available in XSPEC.

5.3. Absorber Masses vs Mass Drop-Out

As suggested in PAPER1 this warm ionized absorber might be the gas that has dropped out of the putative cooling flow during the lifetime of the galaxy or group and thus could provide the confirmation of the inhomogeneous cooling flow scenario that has been suggested to operate in massive elliptical galaxies, groups, and clusters (e.g., Fabian 1994). To make this connection between our measurements of oxygen absorption and the cooling flow scenario we first estimate the mass of absorbing material implied by the measured optical depths. This mass is then compared to the cooling flow mass deposition rate inferred from ASCA data.

Before computing the absorber masses some caveats must be discussed. First, although the simple constant-pressure cooling flow model discussed in §3.6.1 can describe the X-ray emission of the hot gas just as well as the single-phase model, it does not describe the excess 0.2-0.4 keV X-rays presumably arising from the emission of the warm absorbing gas (§3.6.3). Although at this time we cannot exclude the possibility that with a more rigorous treatment of the absorption and emission properties of the warm gas (see end of previous section) that the simple cooling flow model could be compatible with the PSPC data between 0.2-0.4 keV, it is quite possible that an important modification of the simple cooling flow model is required (see §5.5). As a convenient benchmark for comparison to most previous studies we shall consider here the mass deposition rates predicted by the constant-pressure cooling flow models.

Second, the oxygen edge optical depths predicted by the single-edge models without including the emission from the warm gas certainly are overestimates. Recall that when including the warm gas emission in NGC 5044 that τ reduces to a value near the 95% lower limit of the result obtained without including the warm gas emission (§3.6.3). Of equal importance, when including additional edges the inferred optical depth for each edge decreases, and we expect several edges from different ionization states of oxygen, carbon, and nitrogen to contribute (§5.2). Since the absorption of an edge is not linear in the energy of the edge (i.e., $A_0(E) = \exp[-\tau_0(E/E_0)^{-3}]$ and $A_1(E)A_2(E) \neq A_{1+2}(E)$ if the edge energies $E_1 \neq E_2$), by spreading multiple edges over a large energy range one can produce the observed absorption with smaller total optical depth than can be achieved with a single edge. Consequently, the single-edge optical depths obtained in §3.4 should be considered upper limits.

Let us now estimate the amount of absorbing material implied by these absorption measurements with these caveats in mind, and in particular with the assumption that the inferred absorber masses are most likely overestimates. Assuming the optical depths refer to the O_I

TABLE 2
ABSORBER MASSES AND IMPLIED ACCUMULATION TIMESCALES

Name	Central Bin					Total			
	\dot{M} ($M_{\odot}\text{yr}^{-1}$)	R (kpc)	M_{abs} ($10^{10}M_{\odot}$)	t_{acc} (10^{10} yr)	M_{hot} ($10^{10}M_{\odot}$)	R (kpc)	M_{abs} ($10^{10}M_{\odot}$)	t_{acc} (10^{10} yr)	M_{hot} ($10^{10}M_{\odot}$)
N507	$18.50^{+3.50}_{-3.30}$	20.0	$5.86^{+5.85}_{-4.02}$	$0.32^{+0.45}_{-0.23}$	$0.430^{+0.221}_{-0.069}$	200.0	$125.67^{+599.92}_{-92.61}$	$6.79^{+40.94}_{-5.29}$	$43.68^{+12.31}_{-9.41}$
N1399	$1.62^{+0.20}_{-0.18}$	5.2	$0.81^{+0.10}_{-0.62}$	$0.50^{+0.13}_{-0.39}$	$0.019^{+0.012}_{-0.001}$	90.3	$9.41^{+23.11}_{-7.10}$	$5.81^{+16.78}_{-4.54}$	$5.55^{+0.51}_{-0.63}$
N4472	$2.54^{+0.34}_{-0.37}$	5.2	$0.32^{+0.34}_{-0.16}$	$0.12^{+0.27}_{-0.07}$	$0.031^{+0.002}_{-0.018}$	77.2	$47.26^{+39.53}_{-24.67}$	$18.61^{+21.39}_{-10.76}$	$3.65^{+0.36}_{-0.33}$
N4649	$2.20^{+0.30}_{-0.60}$	5.2	$0.35^{+0.41}_{-0.26}$	$0.16^{+0.32}_{-0.13}$	$0.026^{+0.004}_{-0.014}$	36.7	$3.70^{+60.64}_{-3.61}$	$1.68^{+38.53}_{-1.65}$	$0.56^{+0.19}_{-0.25}$
N5044	$41.32^{+4.59}_{-5.42}$	11.0	$1.69^{+1.17}_{-1.13}$	$0.04^{+0.04}_{-0.03}$	$0.266^{+0.052}_{-0.109}$	143.5	$26.52^{+38.17}_{-17.87}$	$0.64^{+1.16}_{-0.45}$	$22.08^{+2.91}_{-4.13}$

NOTE.—Total cooling flow mass deposition rates (\dot{M}) and 90% confidence limits inferred from ASCA data (see text). The quoted errors on M_{abs} refer to 95% confidence limits on τ (“Fix” in Table 1) and assume solar abundances. The accumulation timescale, $t_{\text{acc}} = M_{\text{abs}}/\dot{M}$, reflects both the 95% uncertainties on M_{abs} and the 90% errors on \dot{M} . The mass of hot gas, M_{hot} , and the 95% errors computed within the 3D radius are also given. These values of M_{abs} probably are over-estimates (see beginning of §5.3).

edge, then the measured values of τ imply a hydrogen column density (assuming $\sigma = 5.5 \times 10^{-19} \text{ cm}^2$ at threshold) and thus a mass within a projected radius, R ,

$$M_{\text{abs}}(< R) = (7.8 \times 10^9)(\tau) \left(\frac{R}{10 \text{ kpc}} \right)^2 \left(\frac{\text{O/H}}{8.51 \times 10^{-4}} \right)^{-1} M_{\odot}, \quad (1)$$

where τ is the optical depth of the O I edge and O/H is the oxygen abundance of the absorber. Although the projected mass is larger than the mass within the 3D radius $r = R$, the value of τ in equation (1) slightly underestimates the 3D value as discussed in (§3.2); i.e. these projection effects approximately cancel. The metallicity of the hot gas in the central bins for the objects in our sample are larger than solar (PAPER2), and thus we expect the same for the absorber. Since the oxygen abundance is uncertain we shall quote results assuming O is solar and recognize that M_{abs} could be overestimated by a factor of 2-3 in the central bin. The expected contribution from carbon and nitrogen (§5) to τ also reduces M_{abs} by another $\sim 40\%$.

In Table 2 we give M_{abs} for NGC 507, 1399, 4472, 4649, and 5044 in both the central bin ($R = 1'$) and the total mass interior to the largest bin investigated; the edge optical depths used refer to the single-phase models since the cooling flow models give entirely consistent values (§3.6.1). The mass deposition rates, \dot{M} , listed in the second column are determined from the accumulated ASCA data within radii of $r \sim 3' - 5'$. (The ASCA spectra place much tighter constraints on the total \dot{M} than do the ROSAT spectral data.) The results for NGC 1399, 4472, and 5044 are taken from Buote (1999). For NGC 507 and 4649 we re-analyzed the data sets as prepared in Buote & Fabian (1998) and fitted cooling flow models analogously to that done in Buote (1999). That is, the spectra were fitted with (1) a constant pressure cooling flow component, (2) an isothermal component representing the ambient gas, and (3) for NGC 4649 an extra high-temperature bremsstrahlung component. Since the cooling flow model assumes constant pressure and neglects the gravitational work done on the cooling gas, the value of \dot{M} is an upper limit. This overestimate is typically $\lesssim 30\%$ (e.g., the agreement of different cooling flow models in Allen et al 2000b).

Let us focus on M_{abs} and the accumulation time, $t_{\text{acc}} = M_{\text{abs}}/\dot{M}$, within the central bin ($R = 1'$) where the measured optical depths are most significant and the fits are most clearly improved when the edge is added; i.e. we consider the results for the central bin to be most reliable. Assuming an age of the universe, $t_{\text{age}} = 1.3 \times 10^{10} \text{ yr}$, examination of Table 2 reveals that within the central bin $t_{\text{acc}} \sim (0.1 - 0.5)t_{\text{age}}$ using the best-fitting values or a 95% upper limit of $t_{\text{acc}} \sim (0.3 - 0.6)t_{\text{age}}$; NGC 5044 actually has smaller values, but if the second bin is included (which has intrinsic absorption just as significant as the inner bin) then t_{acc} is consistent with the values quoted above. These accumulation timescales are a sizeable fraction of t_{age} , and thus M_{abs} within the central bin(s) can account for most, if not all, of the mass deposited by the cooling flow over the lifetime of the flow; the exact value depends on precisely when the cooling flow begins and whether \dot{M} varies with time.

The total absorbing masses have large errors within the 95% confidence limits. Although the best-fitting values for t_{acc} are typically larger than t_{age} , the 95% lower limits are $\lesssim t_{\text{age}}$ for all but NGC 4472. We reiterate that we consider these values at the largest radius to be less secure than the central bin(s) because the fits do not clearly require the addition of the oxygen edge outside the inner 1-2 bins. Nevertheless, the result for NGC 4472 is striking and deserves comment. Clearly the approximation of a spherically symmetric, relaxed cooling flow is invalid for $R \gtrsim 3'$ because the isophotal distortions suggest a strong interaction with the surrounding Virgo gas (Irwin & Sarazin, 1996) and thus the estimate of \dot{M} unlikely applies at larger radii. If the large value of M_{abs} at large radius is confirmed then another mechanism must have produced the warm gas in NGC 4472.

Hence, within the central 1-2 bins ($R \sim 10 - 20 \text{ kpc}$) where the model constraints are most secure we conclude that the absorbing mass inferred from the oxygen edges can explain most (and perhaps all) of the mass deposited by a cooling flow over the age of the system. If the edges also apply at larger radii (as we have assumed), then all of the deposited mass (except for NGC 4472) can be easily explained by the inferred absorbing mass. These qualitative conclusions still apply if the oxygen edge optical

depths are really closer to their 95% lower limits as discussed near the top of this section.

We mention that systems without strong cooling flows will not have had sufficient time to accumulate the $\sim 10^9 M_\odot$ within $R \sim 1'$ to produce detectable soft X-ray emission. Thus, the ‘‘Very Soft Components’’ found in galaxies with low ratios of X-ray to optical luminosity unlikely arise from warm gas deposited in a cooling flow and instead probably reflect the collective emission from X-ray binaries (e.g., Irwin & Bregman 1999).

5.4. Constraints from the Optical and FUV

Since collisionally ionized gas at temperatures of 10^{5-6} K emits many strong lines at optical and ultraviolet wavelengths (e.g., Pistinner & Sarazin 1994; Voit & Donahue 1995), we consider whether the large amounts of absorbing material implied by the intrinsic X-ray absorption (Table 2) violate published constraints on line emission in the optical and UV spectral regions. The best published constraints available in the optical are for H α from studies of extended ionized gas in the centers of elliptical galaxies (e.g., Trinchieri & di Alighieri 1991; Goudfrooij et al 1994; Macchetto et al 1996). In most cases the emission line gas is only detected within $r \lesssim 20''$ which is significantly smaller than the central $1'$ used in our analysis.

The object in our sample where H α has been detected out to the largest angular radius is NGC 5044. Macchetto et al (1996) measure $F(\text{H}\alpha) = 1.4 \times 10^{-13} \text{ erg cm}^{-2} \text{ s}^{-1}$ within $R = 0.5'$. We can estimate the temperature at which the H α emission implied by M_{abs} (Table 2) within $R = 1.0'$ equals the observed flux. We take the predicted H α line intensity at peak temperature from Pistinner & Sarazin and the temperature dependence of $\sim T^{-2.5}$ from inspection of Figure 7 of Voit & Donahue. After accounting for the different region sizes we find that the required temperature is $\approx 1.5 \times 10^5$ K using the best-fitting M_{abs} , although when using the 95% lower limit on M_{abs} we find that $T \approx 0.5 \times 10^5$ K.

Similar results hold for NGC 1399, 4472, and 4649 although the comparison is less certain because of the larger aperture corrections. If no aperture correction is made for NGC 5044 then the implied temperatures rise to $T \approx 2.5 \times 10^5$ K at best fit and $T \approx 1.7 \times 10^5$ K at the 95% lower limit. If we consider also that M_{abs} in Table 2 is over-estimated because the oxygen abundance is larger than solar ($\sim 1.5Z_\odot$ – see PAPER2) and carbon and nitrogen contribute $\sim 40\%$ to the measured optical depths (§5.3), we obtain $T \approx 1.8 \times 10^5$ K at best fit and $T \approx 1.2 \times 10^5$ K at the 95% lower limit (again without aperture correction). Therefore, the published constraints on H α are satisfied if $T \gtrsim 2.0 \times 10^5$ K.

Stronger lines from warm gas are expected to appear in the UV, but Hopkins Ultraviolet Telescope (HUT) observations detected no significant emission lines in NGC 1399, 4472, and 4649 (Ferguson et al 1991; Brown, Ferguson, & Davidsen 1995). It is unfortunate that the strongest emission lines for temperatures $T \sim (2 - 3) \times 10^5$ K are O V(1218Å), O VI(1034Å), and N V(1240Å) which appear to be lost in the background geocoronal emission (e.g., Figure 1 of Ferguson et al 1991, though see below for O VI). However, the lines C IV(1549Å), O IV(1401Å), and Ne IV(1602Å) are also strong and uncontaminated by geocoronal emis-

sion.

To determine the gas temperature at which, e.g., the O IV(1401Å) flux would not violate the published UV constraints we estimate that the O IV flux would have to be less than $\sim 10\%$ of the continuum considering the error bars on the spectrum of NGC 1399 (Figure 2 of Ferguson et al 1991). This limit corresponds to a flux of $\sim 1.4 \times 10^{-12} \text{ erg cm}^{-2} \text{ s}^{-1}$. We take the predicted O IV line intensity at peak temperature from Pistinner & Sarazin and assume the temperature gradient above the peak falls similarly to that displayed for C IV in Figure 7 of Voit & Donahue. Using the best-fitting M_{abs} (and accounting for the smaller HUT aperture) we find that a temperature of at least 3×10^5 K is required, though the 95% lower limits on M_{abs} (which are probably more realistic – §3.6.3) coupled with the oxygen abundance and C/N issues as above indicate the limit is more conservatively $\sim 2 \times 10^5$ K. Similar limits are obtained for the other lines and for the HUT spectra of NGC 4472 and 4649 (Brown et al, 1995).

Our procedure of requiring the line fluxes to be less than 10% of the continuum may result in limits that are too restrictive. Dixon et al (1996) have estimated 2σ upper limits on the O VI(1034Å) intensity from M87 which has a HUT spectrum very similar to NGC 1399. Their 2σ upper limit on the O VI flux within a $1'$ circle is $\sim 1 \times 10^{-10} \text{ erg cm}^{-2} \text{ s}^{-1}$. If the warm gas has a temperature of 3.2×10^5 K corresponding to the peak temperature for O VI, then the observed limit is comparable to the O VI emission expected from the warm gas of NGC 1399 when using the 95% lower limit on M_{abs} . Hence, if the HUT results for M87 apply to NGC 1399 (as they appear to), then the predicted O VI emission agrees with the limits, especially if the temperature is not precisely at the peak temperature for O VI.

5.5. Theoretical Issues

Although the hypothesis of warm, mostly collisionally ionized, gas apparently can explain the X-ray observations and the matter deposited by the cooling flows, this model has serious theoretical difficulties which must be overcome before it can be considered a viable model:

1. $T_{\text{warm}} < T_{\text{virial}}$. The temperature of the warm gas ($\lesssim 0.1$ keV) is less than the virial temperatures of the halos (~ 1 keV) implying the gas is not thermally supported. How does the warm gas support itself in the gravitational fields of these systems?
2. $t_{\text{cool}}^{\text{warm gas}} \ll t_{\text{cool}}^{\text{hot gas}}$. The cooling time of the warm gas is very short, even more so than the hot gas in the central regions. How are large quantities of gas maintained at these temperatures?

Most likely these problems can only be solved with a substantial modification of the standard cooling flow scenario. Clearly an additional energy source and very possibly the important role of magnetic fields will have to be considered. A small number of models have been proposed throughout the years which consider these issues, though they are not well developed and do not at present make detailed predictions regarding the issues (1) and (2) above. These models have generally been designed to completely suppress cooling flows, and thus will have to be modified to

allow some cooling of the hot gas. We now briefly review some of the candidate models.

Binney (1996) and Ciotti & Ostriker (2000) have proposed feedback from the central black hole as a promising means of inhibiting the cooling of hot gas in the central regions of galactic cooling flows. In this model whenever the black hole accretes a sufficient amount of gas to stimulate nuclear activity, the accompanying radiation stimulated by the accretion heats up the hot gas and prevents further cooling. This is supposed to be a cyclical process such that the AGN phase is sufficiently rare to be consistent with the lack of nuclear activity in most cooling flows. If the AGN feedback energy does not completely suppress cooling of the hot gas but instead merely prevents most of the gas from cooling down to temperatures below 10^{5-6} K, this might be able to explain issues (1) and (2). We also note that most of the cooling gas is not expected to reach the central black hole in standard models (Brighenti & Mathews, 1999).

Another energy source proposed to exist in the centers of cooling flows is that from the reconnection of tangled magnetic field lines. It has been known for some time that small seed magnetic fields can be amplified within a cooling flow to produce sizeable fields at the centers (e.g., Soker & Sarazin 1990; Lesch & Bender 1990; Moss & Shukurov 1996; Mathews & Brighenti 1997). Zoabi et al (1998) show that reconnection energy can significantly reduce the cooling rates and may account for significant amounts of warm ($T = 10^{5-6}$ K) gas. Similarly, Norman & Meiksen (1996) propose a two-phase model to recycle warm and hot gas along magnetic flux loops also resulting in much lower rates of mass deposition.

Both the AGN and magnetic field reconnection models would explain the warm gas phase as a non-equilibrium configuration where the warm gas is continuously diluted by heating processes and replenished by cooling from the hot phase. If we consider the (unlikely) possibility that the warm gas is a long-lived equilibrium phase (see, e.g., Fabian 1996) then magnetic pressure is probably the most viable non-thermal process which can support the gas. Mathews & Brighenti (1999) describe a possible equilibrium model of the warm gas as the outer envelopes of low mass stars forming in a cooling flow.

The details of how the magnetic field would support the gas are uncertain. Daines et al (1994) suggest that the cool gas blobs would be anchored to the hot gas by the magnetic fields, and thus the pressure support would actually come from the hot gas. However, inspection of Table 2 reveals that $M_{\text{abs}} \sim (1 - 10)M_{\text{hot}}$ within the central bins indicating that the hot gas could not support the cool gas. (The 95% lower limits on M_{abs} are considered here.) At larger radii it may be possible for the hot gas to support the cool gas.

Whatever the details of the magnetic support the condition of hydrostatic equilibrium requires that $B^2 \sim 6M_{\text{abs}}GM_{\text{grav}}r^{-4}$. Using the values for M_{abs} within the central 1' bin quoted in Table 2 and the gravitating masses obtained from previous *ROSAT* studies (David et al 1995; Kim & Fabbiano 1995; Rangarajan et al 1995; Irwin & Sarazin 1996) we find that $B \sim 100\mu\text{G}$ is required within a 5 kpc radius.

Estimates of the magnetic field strengths from radio polarization analyses of these galaxies are lacking, although

there exist estimates using minimum energy arguments for NGC 1399 (Killeen et al, 1988), NGC 4472 (Ekers & Kotanyi, 1977), and NGC 4649 (Stanger & Warwick, 1986) which give consistent results: $B \gtrsim 50 - 100\mu\text{G}$ at the centers and $B \gtrsim (5 - 10)\mu\text{G}$ at $r \sim 0.5'$. Assuming $B \sim r^{-1.2}$ (Mathews & Brighenti, 1997) then these observations imply $\langle B \rangle \sim 5\mu\text{G}$ when averaged over a 1' circle. Since the observations only set lower limits the expected $\langle B \rangle \sim 100\mu\text{G}$ fields are consistent with the observations.

Interestingly, the need for $B \sim 100\mu\text{G}$ in cooling flows has been suggested by Brighenti & Mathews (1997) on entirely different grounds. In their analysis of the gravitating mass distributions of NGC 4472, 4636, and 4649 Brighenti & Mathews (1997) find in every case that the gravitating mass determined from the X-ray analysis falls below that estimated from stellar dynamics for $r \lesssim$ (few)kpc. If $B \sim 100\mu\text{G}$ within the centers of these systems then the X-ray and stellar dynamical masses agree. (A similar result holds for NGC 1399 as well – W. Mathews 2000, private communication.)

Finally, we mention it may be useful to consider a model for the warm gas that does not originate from cooling out of the hot phase. One such possibility is offered by the material continuously ejected by the stars. This material is injected into the ISM with low energy and is shock-heated up to the virial temperature of the halo. Although theoretical arguments suggest that the heating is very rapid (Mathews, 1990), more detailed calculations are required to rule out the possibility that in fact the transition is gradual and could give rise to an observable phase of warm gas consistent with the X-ray observations.

6. CONCLUSIONS

From deprojection analysis of the *ROSAT* PSPC data of 10 cooling flow galaxies and groups with low Galactic columns we have detected oxygen absorption at the $2\sigma/3\sigma$ level intrinsic to the central $\sim 1'$ in half of the sample: NGC 507, 1399, 4472, 4649, and 5044. The data for the other systems are insufficient to place interesting constraints on the absorption profile but are consistent with substantial absorption. We modeled the oxygen absorption as a single edge (rest frame $E = 0.532$ keV) which produces the necessary absorption in both the PSPC and *ASCA* data for $E \gtrsim 0.5$ keV without violating the PSPC constraints over $0.2 \sim 0.4$ keV for which no significant excess absorption is indicated. Assuming the absorber is collisionally ionized gas we infer a temperature of 10^{5-6} K from consideration of the possible edge energies consistent with the PSPC data.

The intrinsic oxygen absorption reconciles the long-standing problem of why negligible column densities for a foreground absorber with solar abundances were inferred from *ROSAT* data whereas large columns were obtained from *ASCA* and other instruments with bandpasses above ~ 0.5 keV. Moreover, since the absorption is confined to energies above ~ 0.5 keV there is no need for large columns of cold H which are known to be very inconsistent with the negligible atomic and molecular H measured in galactic and cluster cooling flows (e.g., Bregman et al 1992; O'Dea et al 1994).

In most of the galaxies and groups we have found that single-phase and cooling flow models cannot explain the

X-ray emission in the soft (0.2-0.4 keV) energy channels of the *ROSAT* PSPC data (§3.6.3). That is, when N_{H} of the standard absorber model is freely fitted it is found that $N_{\text{H}} < N_{\text{H}}^{\text{Gal}}$ in the central bins of most systems, with NGC 4472 and NGC 5044 showing the most significant soft excesses. If we model this soft emission as coronal gas we obtain temperatures 10^{5-6} K in excellent agreement with those inferred from the energy ranges of the absorption edges.

Hence, the sub-Galactic column densities are consistent with a direct detection of the emission from the intrinsic absorbing gas. The agreement between the temperatures inferred from the emission and absorbing properties of the warm gas lends strong support to the ionized gas model. In contrast, dust can not explain the excess soft X-ray emission. (Other problems exist with the dust hypothesis – see §5.1.)

Our simple estimates of the amount of absorbing matter implied by our single-edge absorption measurements are consistent with the total amount of matter expected to have been deposited by a cooling flow (§5.3). With the arrival of higher quality data from *Chandra* and *XMM* more accurate estimates should be made which account for a range of absorbing edges and possible radiative transfer effects in the warm gas.

We have examined the theoretical difficulties associated with attributing the absorption to warm ionized gas and have discussed some candidate models that may be able to account for these problems. Future detailed calculations are required to assess the viability of these models (§5.5).

Fortunately on the observational front it will be very easy to verify the intrinsic oxygen absorption with new *Chandra* and *XMM* data. The *XMM* (EPIC) and *Chandra* (ACIS-S) CCDs both extend down to 0.1-0.2 keV and have substantially better energy resolution than the PSPC. Observations with these instruments can easily test our prediction for warm gas in both absorption and emission. The grating spectrometers of *XMM* and *Chandra* have even better energy resolution (but smaller effective area) and, in principle, might detect individual edges.

We emphasize that the absorption signature of the warm gas is expected to be a relatively broad trough over ener-

gies 0.4 ~ 0.8 keV, and thus future *Chandra* and *XMM* observations will not see a single sharp feature. The most straightforward means to confirm our results will be to reproduce the sensitivity of N_{H} to E_{min} for a standard absorber model (§3.3). To obtain the properties of the absorber (e.g., temperature and abundances) a model for the soft X-ray opacity such as that described by Krolik & Kallman (1984) must be compared to the new data. In so doing the emission from the warm gas must also be accounted for (§3.6.3), and thus it is very important that the detector bandpass extend down to ~ 0.1 keV which it does for the *Chandra* and *XMM* CCDs.

As discussed in §5.4 optical and FUV constraints imply a lower limit of $T \sim 2 \times 10^5$ K. It is possible that precise measurements of O III(5007Å) could refine this limit, but since this line peaks at $T \sim 0.8 \times 10^5$ K its emissivity is already falling rapidly at $T \sim 2 \times 10^5$ K. Future high resolution FUV spectroscopy of the O VI (1034Å) line (peak temperature 3.2×10^5 K) with, e.g., FUSE may be able to place additional interesting constraints on the warm gas if its temperature does not exceed $T \approx 5 \times 10^5$ K.

It should be remembered that to infer the properties of the warm gas from X-ray observations the absorption and emission spectrum arising from warm gas must be disentangled from Galactic absorption and the emission from hot plasma. Since (if confirmed) the warm gas almost certainly represents the mass deposited by an inhomogeneous cooling flow (§5.3), the hot gas at each radius should also emit over a range of temperatures. Hence, the thermodynamic state of the X-ray emitting plasma appears to be very complex in the central regions of the (X-ray) brightest galaxies and groups, and the analogous results for A1795 presented in PAPER1 suggest the same applies for galaxy clusters.

I thank W. Mathews for fruitful discussions and the anonymous referee for detailed comments. Support for this work was provided by NASA through Chandra Fellowship grant PF8-10001 awarded by the Chandra Science Center, which is operated by the Smithsonian Astrophysical Observatory for NASA under contract NAS8-39073.

REFERENCES

- Allen, S. W., & Fabian, A. C. 1997, MNRAS, 286, 583
 Allen, S. W., Di Matteo, T., & Fabian, A. C., 2000a, MNRAS, in press (astro-ph/9910188)
 Allen, S. W., Fabian, A. C., Johnstone, R. M., & Nulsen, P. E. J., 2000b, MNRAS, submitted (astro-ph/9910188)
 Arabadjis, J. S., & Bregman, J. N., 1999, ApJ, 514, 607
 Arnaud, K. A., & Mushotzky, R. F., 1998, ApJ, 501, 119
 Balucińska-Church, M., & McCammon, D., 1992, ApJ, 400, 699
 Bevington, P. R., 1969, Data Reduction and Error Analysis for the Physical Sciences. (New York: McGraw-Hill)
 Binney, J. J., 1996, in Gravitational Dynamics Proc. 36th Herstmonceux conf., ed O. Lahav (Cambridge: Cambridge University Press), 89
 Bregman, J. N., Hogg, D. E., & Roberts, M. S., 1992, ApJ, 387, 484
 Briel, U. G., & Henry, J. P., 1996, ApJ, 472, 131
 Brighenti, F., & Mathews, W. G., 1997, ApJ, 486, L83
 Brighenti F., & Mathews W. G., 1998, ApJ, 495, 239
 Brighenti F., & Mathews W. G., 1999, ApJ, 527, L89
 Brown, T. M., Ferguson, H. C., Davidsen, A. F., 1995, ApJ, 454, L15
 Buote, D. A., 1999, MNRAS, 309, 695
 Buote, D. A., 2000a, MNRAS, 311, 176
 Buote, D. A., 2000b, ApJ, 532, L113 (PAPER1)
 Buote, D. A., 2000c, ApJ, in press (PAPER2) (astro-ph/0001329)
 Buote, D. A., & Fabian, A. C. 1998, MNRAS, 296, 977
 Buote, D. A., Canizares, C. R., & Fabian, A. C. 1999, MNRAS, 310, 483
 Ciotti, L., & Ostriker, J. P., 2000, ApJ, submitted (astro-ph/9912064)
 Daines, S. J., Fabian, A. C., & Thomas, P. A., 1994, MNRAS, 268, 1060
 Daltabuit, E., & Cox, D. P., 1972, ApJ, 177, 855
 David, L. P., Jones, C., Forman, W., Daines, S., 1994, ApJ, 428, 544
 Dickey J. M., Lockman F. J., 1990, ARA&A, 28, 215
 Dixon, W., Hurwitz, M., & Ferguson, H. C., 1996, ApJ, 469, L77
 Ekers, R. D., & Kotanyi, C. G., 1977, A&A, 67, 47
 Fabian A. C., 1994, ARA&A, 32, 277
 Fabian A. C., 1996, Science, 271, 1244
 Fabian, A. C., Arnaud, K. A., Bautz, M. W., & Tawara, Y., 1994, ApJ, 436, L63
 Ferguson, H. C., et al. 1991, ApJ, ApJ, 382, L69
 Forman W., Jones C., David L., Franx M., Makishima K., & Ohashi T., 1993, ApJ, 418, L55
 Goudfrooij, P., Hansen, L., Jorgensen, H. E., & Norgaard-Nielsen, H. U., 1994, A&AS, 105, 341
 Gould, R. J., & Jung, Y.-D., 1991, ApJ, 373, 271
 Ikebe Y., et al., 1997, ApJ, 481, 660
 Irwin, J. A., & Bregman, J. N., 1999, ApJ, 527, 125
 Irwin, J. A., & Sarazin, C. L., 1996, ApJ, 471, 663

- Johnstone R. M., Fabian A. C., Edge A. C., & Thomas P. A., 1992, *MNRAS*, 255, 431
- Jones, C., Stern, C., Forman, W., Breen, J., David, L., Tucker, W., & Franx, M., 1997, *ApJ*, 482, 143
- Killeen, N. E. B., Bicknell, G. V., & Ekers, R. D., 1988, *ApJ*, 325, 180
- Kim, D.-W., & Fabbiano, G., 1995, *ApJ*, 441, 182
- Krolik, J. H., & Kallman, T. R., 1984, *ApJ*, 286, 366
- Laor, A., & Draine, B. T., 1993, *ApJ*, 402, 441
- Lesch, H., & Bender, R., 1990, *A&A*, 233, 417
- Lester, D. F., Zink, E. C., Doppmann, G. W., Gaffney, N. I., Harvey, P. M., Smith, B. J., & Malkan, M., 1995, *ApJ*, 439, 185
- Macchetto, F., Pastoriza, M., Caon, N., Sparks, W. B., Giavalisco, M., Bender, R., & Capaccioli, M., 1996, *A&AS*, 120, 463
- Mathews, W. G., 1990, *ApJ*, 354, 468
- Mathews, W. G., & Brighenti, F., 1997, *ApJ*, 488, 595
- Mathews, W. G., & Brighenti, F., 1999, *ApJ*, 526, 114
- Morrison, R., & McCammon, D., 1983, *ApJ*, 270, 119
- Moss, D., & Shukurov, A., 1996, *MNRAS*, 279, 229
- Nahar, S. N., 1999, *ApJS*, 120, 131
- Nahar, S. N., & Pradhan, A. K., 1997, *ApJS*, 111, 339
- Norman, C., & Meiksen, A., 1996, *ApJ*, 468, 97
- O'Dea, C. P., Baum, S. A., Maloney, P. R., Tacconi, L. J., Sparks, W. B., 1994, *ApJ*, 422, 467
- Pistinner, S., Sarazin, C. L., 1994, *ApJ*, 433, 577
- Rangarajan, F. V. N., Fabian, A. C., Forman, W. R., & Jones, C., 1995, *MNRAS*, 272, 665
- Sarazin, C. L., Wise, M. W., Markevitch, M. L., 1998, *ApJ*, 498, 606
- Snowden, S. L., McCammon, D., Burrows, D. N., & Mendenhall, J. A., 1994, *ApJ*, 424, 714
- Soker, N., & Sarazin, C. L., 1990, *ApJ*, 348, 73
- Stanger, V. J., & Warwick, R. S., 1986, *MNRAS*, 220, 363
- Sutherland, R. S., & Dopita, R. S., 1993, *ApJS*, 88, 253
- Thomas P. A., Fabian A. C., & Nulsen P. E. J., 1987, *MNRAS*, 228, 973
- Trinchieri, G., & di Serego Alighieri, S., 1991, *AJ*, 101, 1647
- Trinchieri G., Fabbiano G., Kim D.-W., 1997, *A&A*, 318, 361
- Trinchieri G., Kim D.-W., Fabbiano G., & Canizares C., 1994, *ApJ*, 428, 555
- Tsai, J. C., & Mathews, W. G., 1995, *ApJ*, 448, 84
- Tsai, J. C., & Mathews, W. G., 1996, *ApJ*, 468, 571
- Voit, G. M., & Donahue, M., 1995, *ApJ*, 452, 164
- White, D. A., Fabian A. C., Johnstone R. M., Musthotzky, R. F., & Arnaud, K. A., 1991, *MNRAS*, 252, 72
- Xu H., Makishima K., Fukazawa Y., Ikebe Y., Kikuchi K., Ohashi T., & Tamura T., 1998, *ApJ*, 500, 738
- Zoabi, E., Soker, N., & Regev, O., 1998, *MNRAS*, 296, 579